Interaction between an elastic wave and a single pinned dislocation

Agnès Maurel,[1] Vincent Pagneux,[2] Felipe Barra,[3] and Fernando Lund[3,4]
[1]*Laboratoire Ondes et Acoustique, UMR CNRS 7587, Ecole Supérieure de Physique et de Chimie Industrielles, 10 rue Vauquelin, 75005 Paris, France*
[2]*Laboratoire d'Acoustique de l'Université du Maine, UMR CNRS 6613 Avenue Olivier Messiaen, 72085 Le Mans Cedex 9, France*
[3]*Departamento de Física, Facultad de Ciencias Físicas y Matemáticas, Universidad de Chile, Casilla 487-3, Santiago, Chile*
[4]*Centro para la Investigación Interdisciplinaria Avanzada en Ciencias de los Materiales (CIMAT), Santiago, Chile*
(Received 2 June 2005; revised manuscript received 19 September 2005; published 11 November 2005)

Acoustic, and more generally elastic, waves in solids are damped by several mechanisms, among which dislocation motion is believed to play an important role. This is because an elastic wave interacts with a dislocation causing it to oscillate in response, and the resulting transfer of energy from wave to dislocation damps the acoustic vibrations. Recently, improved experimental techniques as well as improved numerical methods have been able to probe in some detail this interaction, isolating the effect of a single dislocation, and at this stage the theory, in its analytic form, is not sufficiently developed to provide quantitative comparison with experimental data and computer simulations. There is thus a need for an improved theoretical study of this issue. In this paper, we consider the interaction of transverse (T) and longitudinal (L) polarized waves in a homogeneous and isotropic, three dimensional, continuum linear elastic medium interacting with a dislocation segment pinned at both ends. An elastic wave incident upon such a dislocation segment is scattered, and the resulting scattered wave is characterized by its scattering amplitudes, that account for possible T-L mode conversions. Such scattering amplitudes are explicitly calculated. As a consequence, it is possible to calculate the resulting interference patterns of incident with scattered wave, such as have been observed in recent experiments [Shilo and Zolotoyabko, Phys. Rev. Lett. **91**, 115506 (2003)]. The energy loss per cycle is also calculated using the optical theorem and results are shown to be in qualitative agreement with the results of numerical experiments [Greaney *et al.*, Comput. Mater. Sci. **25**, 387 (2002)].

DOI: 10.1103/PhysRevB.72.174110 PACS number(s): 61.72.Lk, 72.10.Fk, 62.20.−x, 81.70.Cv

I. INTRODUCTION

Acoustic, or elastic, waves in solids are damped by several mechanisms, among which dislocation motion is believed to play an important role. Consequently, measurements of ultrasound attenuation in solids have been used for many years as a nonintrusive probe of those mechanical properties of materials that are determined by dislocation behavior (see references in Ref. 1), and there are many ongoing efforts to better understand the dynamics of dislocations, especially the interaction between a wave and a single dislocation. In recent years, improvements in experimental and computational techniques have provided a strong motivation to improve the existing theoretical understanding. Indeed, these works provide measurements with sufficient accuracy so they can be used to examine on a quantitative basis the theoretical models. The interaction of an elastic wave with a single dislocation segment has been studied recently in the experiments of Shilo and Zolotoyabko.[2–4] Using a technique of stroboscopic x-ray imaging, they are able to visualize the scattered wave front in a way so precise that it is possible to make quantitative measurements. Their various experiments have been performed for different incidences of the wave on the dislocation segment, so that a correct interpretation of their results necessitates a theory that captures the vector character of the problem in terms of the various polarizations of the elastic wave as well as the orientation of the segment with respect to the direction of propagation of the incident wave. In numerical experiments, Greaney *et al.*[5,6] have studied the motion of a pinned dislocation segment and have measured the energy loss per cycle for a single dislocation, as opposed to attenuation due to multiple dislocation segments.

The basic mechanism of the elastic wave-dislocation interaction was proposed in 1951 by Nabarro,[7] who noted that waves would be scattered by a dislocation because the motion induced by the incoming wave would generate the emission of a scattered wave. Thus, the mechanism involves two steps, first, the motion of a dislocation in the presence of an incident wave must be determined, and second, a representation of the elastic field generated by a moving dislocation must be obtained. The pioneer works of the 1950s tackled this problem using an electromagnetic analogy that is useful in the case of a screw dislocation in interaction with an antiplane shear wave in two dimensions, which is a scalar problem.[7–9] However, this analogy is no longer valid when considering both longitudinal and transverse waves, each one with its own propagation velocity. In 1963, Mura[10] derived from the Navier equations an integral representation for the elastic field generated by a dislocation loop in three dimensions in arbitrary motion, of which the case of an edge dislocation studied by Kiusalaas[11] is a particular case. The derivation from the Navier equation of the equation of motion for a dislocation in the presence of an external time-dependent stress is due to Lund[12] in 1988 on the observation that the equations of dynamic elasticity follow from a variational principle. This work, together with the integral representation of Mura[10] provides the two steps needed for a full description of the scattering of elastic waves by dislocations in three dimensional elastic media, as Nabarro anticipated. In

a previous study, we have tackled the two dimensional problem for both screw and edge dislocations[13] and the results have been shown to be in agreement with previous particular cases mentioned above.[7–9,11]

A similar approach, i.e., involving the two steps of the interaction, was developed during the 1950s to the 1980s by Granato, Lücke, and co-workers.[14–18] However, as discussed in Ref. 1 their model applies within the framework of an effective medium where the solution for the elastic field is a plane wave, as opposed to a scattered wave, with spherical wave fronts in the far field, expected when a single dislocation is considered. This plane wave solution corresponds to the so-called coherent wave resulting from a multiple scattering process averaged over all realizations of the disordered medium. This approach has been used in the case of an ensemble of random distributed bidimensional[19] and three dimensional[1] dislocations. In addition, the Granato-Lücke approach considers a scalar model that certainly captures the essence of the physics of the interaction between an elastic wave and a random ensemble of dislocations but it does not consider the many complexities due to the vector nature of the variables involved in this interaction. For example, it does not differentiate between edge and screw dislocations, nor among the various polarizations available to an elastic wave.

In a previous paper,[13] we have described the interaction of an elastic wave with a point dislocation in two dimensions and in the limit of low temperatures where drag forces can be neglected. The aim of this preliminary work was to describe the theoretical framework in which the elastic wave-dislocation interaction can be fully described. However, the scattering cross section laws were divergent at low frequencies because of the bidimensionality and a quantitative comparison with, say, experimental values of energy losses, was not possible. The main purpose of the present paper is to extend our previous study to the case of three dimensions and to include internal friction effects that are present in real problems.

The paper is organized as follows: Section II presents the basic equations of the motion of a dislocation segment with pinned ends submitted to an external oscillatory stress, and the scattered wave due to dislocation motion. We consider small amplitudes of the external stress, so that the model is linear. For instance, the external stress is small enough to maintain the segment of dislocation firmly anchored at the two endpoints and possible formation of dislocation under Frank-Read mechanism is not considered.[20] It will be assumed that the motion is subsonic and that the wavelength of the incident wave $2\pi/k$ ($k=k_T$, k_L for transverse and longitudinal waves, respectively) is large compared to the segment length L and to the amplitude of dislocation motion, introducing a small parameter kL for this scattering problem.

Section III presents the derivation of the scattering amplitudes that characterize the angular dependence of the scattered waves for given orientations of both the dislocation segment and the incident wave. This is done in a first Born approximation, allowing us to obtain all elastic fields. An illustrative example is given for the interference pattern observed when the scattered wave superposes to the incident wave, as it could be observed in numerical experiments and it is here qualitatively compared with the interference pattern experimentally obtained in Refs. 2 and 3. Section IV formulates an optical theorem for polarized waves. This allows us to calculate the energy loss by the incident wave due to scattering per cycle, and the particular case numerically studied in Refs. 5 and 6 is taken as example for comparison. In Sec. V we present some concluding remarks. Some technical calculations are collected in three appendixes.

II. BASIC EQUATIONS

In the rest of the paper, we adopt the following notations: (λ,μ) are the Lamé constants and ρ is the density of an infinite, homogeneous, and isotropic medium, $c_L \equiv \sqrt{(\lambda+2\mu)/\rho}$, $c_T \equiv \sqrt{\mu/\rho}$ denote the velocities of the longitudinal and transverse elastic waves, respectively, and $\gamma \equiv c_L/c_T$. σ denotes the stress tensor, with $\sigma_{ij}=c_{ijkl}\partial u_k/\partial x_l$, the vector $\mathbf{u}$ is the elastic displacement and $c_{ijkl}=\lambda\delta_{ij}\delta kl + \mu(\delta_{ik}\delta_{jl}+\delta_{il}\delta_{jk})$ is the elastic constants tensor. We shall use also the velocity $\mathbf{v}$, the time derivative of the displacement $\mathbf{u}$. The dislocation segment position is denoted $\mathbf{X}(s,t)$ and it is locally oriented with a unit vector $\boldsymbol{\tau} \equiv \mathbf{X}'/|\mathbf{X}'|$, where prime denotes the derivative with respect to the Lagrangian parameter s. Time derivatives will be denoted by an overdot. The dislocation between the two pinning points is assumed to be straight at equilibrium (i.e., unbiased) with length L. In addition, the wavelength of the incident wave $2\pi/k$ ($k=k_L$, k_T for the longitudinal or transverse polarizations) is assumed to be large compared to both (i) the length L of the dislocation segment and (ii) the amplitude of the dislocation motion. Thus, we can consider $\boldsymbol{\tau}$ as the unit vector along the direction of the segment at equilibrium. With $\mathbf{X}_0$ the center of the dislocation segment at equilibrium, we also get $k|\mathbf{X}(s,t) - \mathbf{X}_0| \sim kL \ll 1$. We shall also assume that the dislocation line oscillates at velocities low compared with c_L, c_T (subsonic hypothesis), and we do not consider nonlinear scattering effects (phonon wind[21]) (see Fig. 1).

Finally, we consider a gliding edge dislocation segment, so that $\dot{\mathbf{X}}$ and the Burgers vector $\mathbf{b}$ are parallel for small amplitude motion (the unit vector $\mathbf{t}$ denotes their common direction) and both are perpendicular to $\boldsymbol{\tau}$. We define the unit vector $\mathbf{n} \equiv \boldsymbol{\tau} \times \mathbf{t}$.

The mechanism for the wave scattering is the following: the incident wave hits the dislocation, causing it to oscillate in response. The ensuing oscillatory motion generates outgoing (from the dislocation position) elastic waves. The goal of this section is to derive the equation of motion of an edge dislocation line with pinned ends. This equation is then coupled with an equation for the wave generated by the motion of the dislocation segment.

Before going further, let us remark that the study presented in this section is performed on a single segment but it can be extended to a fragmented dislocation line as pictured in Fig. 2 from the representation of Refs. 14, 22, and 23. In that representation, a dislocation network, of total length L_N is fragmented into smaller segments of length L because of high concentration of pinning points such as impurity atoms. The pinning points can be fixed points or they can move as pictured in Ref. 17. More generally, any given configuration

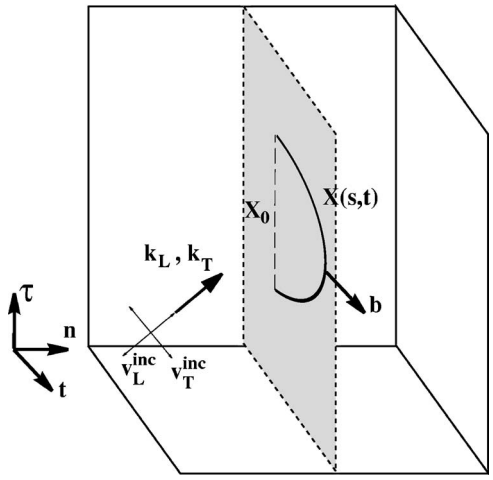

FIG. 1. Configuration of the dislocation segment anchored at both extremities bowing under the action of an external stress that results in the propagation of a transverse (T) and longitudinal (L) waves (dislocation bow out is exaggerated for the sake of clarity). $v_{L,T}^{\mathrm{inc}}$ denote the velocities associated with the external stress, $k_{L,T}$ the corresponding wave vectors. $\mathbf{X}(s,t)$ denotes the current position along the bowed line, $\mathbf{X}_0$ the center of the segment at equilibrium.

of dislocation segments can be treated by superposition of the elementary solution that is the object of the present section. Only a random configuration necessitates a change in the mathematical treatment.[1,19]

A. Equation of motion of a pinned dislocation segment

We consider a dislocation segment moving at low velocities, $\dot{X} \ll c_L$, c_T with pinned ends. Low accelerations are also assumed, so that the back-reaction of the radiation on the dislocation dynamics can be neglected. Following Ref. 12 and under these hypothesis, the equation of motion of an edge dislocation takes the form of the equation of motion for a string endowed with mass and line tension, forced by the usual Peach-Koehler force[24,25]

$$m\ddot{X}_k(s,t) + B\dot{X}_k(s,t) - \Gamma X_k''(s,t) = F_k(t), \tag{2.1}$$

and the associated boundary conditions at pinned ends $X_k(\pm L/2,t)=0$. In Eq. (2.1),

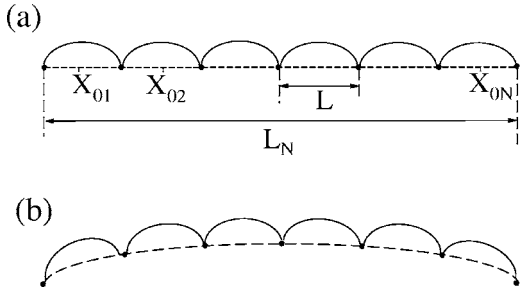

FIG. 2. Dislocation network of length L_N fragmented into smaller segments with pinned ends. The pinners can be fixed (a) or movable with the network (b).

$$m \equiv \frac{\rho b^2}{4\pi}(1+\gamma^{-4})\ln(\delta/\delta_0), \tag{2.2}$$

defines a mass per unit length (with δ, δ_0 the long- and short-distance cutoff lengths, respectively) and

$$\Gamma \equiv \frac{\rho b^2}{2\pi}(1-\gamma^{-2})c_T^2 \ln(\delta/\delta_0) \tag{2.3}$$

is the line tension, B is the drag coefficient (for a detailed discussion on the drag, see Ref. 21) and $F_k = \epsilon_{kjm}\tau_m b_i \sigma_{ij}$ the Peach-Koehler force (ϵ_{ijk} denotes the usual completely antisymmetric tensor).

This equation of motion is projected onto the glide direction $\mathbf{t}$, and we get, for the line velocity $\dot{X}=\dot{X}_k t_k$ (where repeated indices imply summation)

$$m\ddot{X}(s,t) - \Gamma X''(s,t) = \mu b\, \mathsf{M}_{lk}\partial_l u_k(\mathbf{X},t) - B\dot{X}(s,t), \tag{2.4}$$

with

$$\mathsf{M}_{lk} \equiv t_l n_k + t_k n_l. \tag{2.5}$$

Equation (2.4) is solved using $\mathbf{u}(\mathbf{X},t) \simeq \mathbf{u}(\mathbf{X}_0,t)$ in the term of the Peach-Koehler force, a valid approximation for low amplitude motion. In the harmonic regime $e^{i\omega t}$, we get

$$-(m\omega^2 + i\omega B)X(s,\omega) - \Gamma X''(s,\omega) = \mu b \mathsf{M}_{lk}\partial_l u_k(\mathbf{X}_0,\omega), \tag{2.6}$$

whose solution, using the velocity $\mathbf{v}(\mathbf{x},\omega) = -i\omega\mathbf{u}(\mathbf{x},t)$, is

$$\dot{X}(s,\omega) = -\frac{4}{\pi}\frac{\mu b}{m}\tilde{S}(s,\omega)\mathsf{M}_{lk}\partial_l v_k(\mathbf{X}_0,\omega), \tag{2.7}$$

with

$$\tilde{S}(s,\omega) = \sum_{N\ \mathrm{odd}} \frac{1}{N(\omega^2 - \omega_N^2 + i\omega B/m)} \sin\left(\frac{N\pi}{L}(s+L/2)\right), \tag{2.8}$$

and

$$\omega_N = N\omega_1, \quad \text{with } \omega_1 \equiv \sqrt{\frac{\Gamma}{m}}\frac{\pi}{L}. \tag{2.9}$$

Let us remark that, when kL is small, $\omega_1 \simeq \omega(\pi/kL) \gg \omega$ so that the sum in Eq. (2.8) can be approximated by the first term,

$$\tilde{S}(s,\omega) \simeq \frac{1}{\omega^2 - \omega_1^2 + i\omega B/m} \sin\left(\frac{\pi}{L}(s+L/2)\right).$$

The motion will be over-damped if $B/2m\omega_1$ is larger than one. This condition is roughly in agreement with the usual critical value of the drag coefficient[21,26]

$$B_c = 2\pi\Gamma/(c_T L), \tag{2.10}$$

above which the dislocation motion becomes overdamped.

Equation (2.7) gives the displacement of the dislocation line if the elastic displacement of the incident wave [through the term $v_k(\mathbf{X}_0,\omega)$] is known. Note that Weertman[27] obtained an analytical solution for $X(s,t)$. Equations (2.7) and (2.8)

correspond to the Fourier series expansion of Weertman's solution. This representation allows us to obtain easily $X(s,t)$ in the long wavelength limit.

Next, an equation for the scattered wave is necessary. This is the object of the following section.

B. Integral representation for the scattered wave

The elastic wave scattered by a moving dislocation can be derived using the wave equation and the discontinuity relation $[\mathbf{u}]=\mathbf{b}$, first given in Ref. 10 (see also Ref. 19). An integral representation is obtained for the scattered velocity,

$$v_m^s(\mathbf{x},t) = \epsilon_{jnh} c_{ijkl} \int\int_{\mathcal{L}} dt'\, ds\; b_i \dot{X}_n(s,t')\, \tau_h \frac{\partial}{\partial x_l} \times G^0_{km}(\mathbf{x}-\mathbf{X}_0, t-t'), \tag{2.11}$$

where $\mathcal{L}$ represents the dislocation segment of length L and where the Green tensor of free space G^0 verifies

$$\rho \frac{\partial^2}{\partial t^2} G^0_{im}(\mathbf{x},t) - c_{ijkl} \frac{\partial^2}{\partial x_j\, \partial\, x_l} G^0_{km}(\mathbf{x},t) = \delta(\mathbf{x})\,\delta(t)\,\delta_{im}. \tag{2.12}$$

In the integral representation above, $\mathbf{X}_0$ has been used instead of $\mathbf{X}(s,t)$. An exact form of the Green tensor can be found in Refs. 11 and 28. Its asymptotic form for large x is

$$G^0_{ij}(\mathbf{x},\omega) \simeq \frac{1}{4\pi\rho}\left(\frac{\mathsf{P}_{\hat{\mathbf{x}}ij}}{c_L^2} \frac{e^{ik_L x}}{x} + \frac{(\mathsf{I}-\mathsf{P}_{\hat{\mathbf{x}}})_{ij}}{c_T^2} \frac{e^{ik_T x}}{x} \right),$$

where $\mathsf{P}_{\hat{\mathbf{x}}ij} \equiv \hat{x}_i \hat{x}_j$ and $\mathsf{I}-\mathsf{P}_{\hat{\mathbf{x}}}$ are the projectors along the directions parallel and perpendicular to $\hat{\mathbf{x}}$ respectively, and with $k_a=\omega/c_a$, $c_a=c_L$, c_T.

III. SCATTERED ELASTIC FIELD

We calculate in this section the scattered field resulting from the interaction of the elastic wave with a pinned dislocation. This is done through the derivation of the scattering amplitudes defined in Eq. (3.5) below, that account for possible mode conversions. From the scattering amplitudes, the elastic fields can be obtained and an example is provided.

A. Scattering amplitudes

The integral representation of the scattered wave in Eq. (2.11) is written substituting the solution $\dot{X}$ for the dislocation velocity in Eq. (2.7). In the frequency domain, we get

$$v_m^s(\mathbf{x},\omega) = \frac{8L}{\pi^2} \frac{\mu b}{m} \frac{S(\omega)}{\omega^2} c_{ijkl}\, t_i\, n_j \frac{\partial}{\partial x_l} G^0_{km}(\mathbf{x},\omega) \mathsf{M}_{np} \partial_n v_p(\mathbf{X}_0,\omega),$$

where we have used $\epsilon_{jnh} \dot{X}_n \tau_h = -\dot{X} n_j$ and with

$$S(\omega) \equiv \frac{\pi\omega^2}{2L} \int_{-L/2}^{L/2} ds\; \tilde{S}(s,\omega) \simeq \frac{\omega^2}{\omega^2 - \omega_1^2 + i\omega B/m}. \tag{3.1}$$

Using $c_{ijkl} b_i n_j = \mu b \mathsf{M}_{lk}$ [M is defined in Eq. (2.5)], we get

$$v_m^s(\mathbf{x},\omega) = \frac{2i}{\pi^3}\left(\frac{\rho b^2}{m}\right) \frac{S(\omega)}{\omega} c_T^4 L \frac{x_l}{x^2} \mathsf{M}_{lk} \left(\frac{\mathsf{P}_{\hat{\mathbf{x}}km}}{c_L^3} e^{ik_L x} + \frac{(\mathsf{I}-\mathsf{P}_{\hat{\mathbf{x}}})_{km}}{c_T^3} e^{ik_T x} \right) \mathsf{M}_{np} \partial_n v_p(\mathbf{X}_0,\omega). \tag{3.2}$$

The scattering amplitudes are determined in a first Born approximation, with $\mathbf{v}=\mathbf{v}^{\mathrm{inc}}$ on the right-hand side term of Eq. (3.2).

The general form of an incident wave propagating in the $\hat{\mathbf{k}}_0$ direction is given by

$$\mathbf{v}^{\mathrm{inc}}(\mathbf{x},\omega) = A_L e^{i\mathbf{k}_L \mathbf{x}} \hat{\mathbf{k}}_0 + A_T e^{i\mathbf{k}_T \mathbf{x}} \hat{\mathbf{y}}_0, \tag{3.3}$$

where both longitudinal and transverse polarizations, of amplitudes A_L and A_T, and directions $\hat{\mathbf{k}}_0$ and $\hat{\mathbf{y}}_0$, respectively ($\hat{\mathbf{y}}_0 \cdot \hat{\mathbf{k}}_0 = 0$) are considered.

The scattered wave is similarly split, $\mathbf{v}^s = \mathbf{v}_L^s + \mathbf{v}_T^s$, where $\mathbf{v}_L^s$ is the longitudinal scattered wave (parallel to the $\hat{\mathbf{x}}$ direction) and $\mathbf{v}_T^s$ is the transverse scattered wave (parallel to a $\hat{\mathbf{y}}$ direction with $\hat{\mathbf{y}} \cdot \hat{\mathbf{x}} = 0$). Using Eq. (3.2), it is easily found that

$$\mathbf{v}_L^s(\mathbf{x},\omega) = -\frac{2}{\pi^3}\left(\frac{\rho b^2}{m}\right)\left(\frac{c_T}{c_L}\right)^4 L\; S(\omega) \times \mathsf{P}_{\hat{\mathbf{x}}} \mathsf{N}\left(A_L \hat{\mathbf{k}}_0 + \frac{c_L}{c_T} A_T \hat{\mathbf{y}}_0 \right) \frac{e^{ik_L x}}{x},$$

$$\mathbf{v}_T^s(\mathbf{x},\omega) = -\frac{2}{\pi^3}\left(\frac{\rho b^2}{m}\right) L\; S(\omega) (\mathsf{I}-\mathsf{P}_{\hat{\mathbf{x}}}) \times \mathsf{N}\left(\frac{c_T}{c_L} A_L \hat{\mathbf{k}}_0 + A_T \hat{\mathbf{y}}_0 \right) \frac{e^{ik_T x}}{x}, \tag{3.4}$$

where $\mathsf{N} \equiv \mathsf{M} \hat{\mathbf{x}}^t \hat{\mathbf{k}}_0 \mathsf{M}$ is an operator that depends on the direction $\hat{\mathbf{x}}$ of the scattered wave, and on the direction $\hat{\mathbf{k}}_0$ of the incident wave. The scattering amplitudes f, defined as the angular response of the scatterer

$$\mathbf{v}_L^s(\mathbf{x},\omega) = [f_{LL}(\hat{\mathbf{x}}) A_L + f_{LT}(\hat{\mathbf{x}}) A_T] \frac{e^{ik_L x}}{x} \hat{\mathbf{x}},$$

$$\mathbf{v}_T^s(\mathbf{x},\omega) = [f_{TL}(\hat{\mathbf{x}}) A_L + f_{TT}(\hat{\mathbf{x}}) A_T] \frac{e^{ik_T x}}{x} \hat{\mathbf{y}},$$

are then simply obtained by identification with Eq. (3.4). The result is

$$f_{LL}(\hat{\mathbf{x}}) = -\frac{2}{\pi^3}\left(\frac{\rho b^2}{m}\right) \gamma^{-4}\; L\, S(\omega)\; f_L(\hat{\mathbf{k}}_0) g_L(\hat{\mathbf{x}}),$$

$$f_{LT}(\hat{\mathbf{x}}) = -\frac{2}{\pi^3}\left(\frac{\rho b^2}{m}\right) \gamma^{-3}\; L\, S(\omega)\; f_T(\hat{\mathbf{k}}_0) g_L(\hat{\mathbf{x}}),$$

$$f_{TL}(\hat{\mathbf{x}}) = -\frac{2}{\pi^3}\left(\frac{\rho b^2}{m}\right) \gamma^{-1}\; L\, S(\omega)\; f_L(\hat{\mathbf{k}}_0) g_T(\hat{\mathbf{x}}),$$

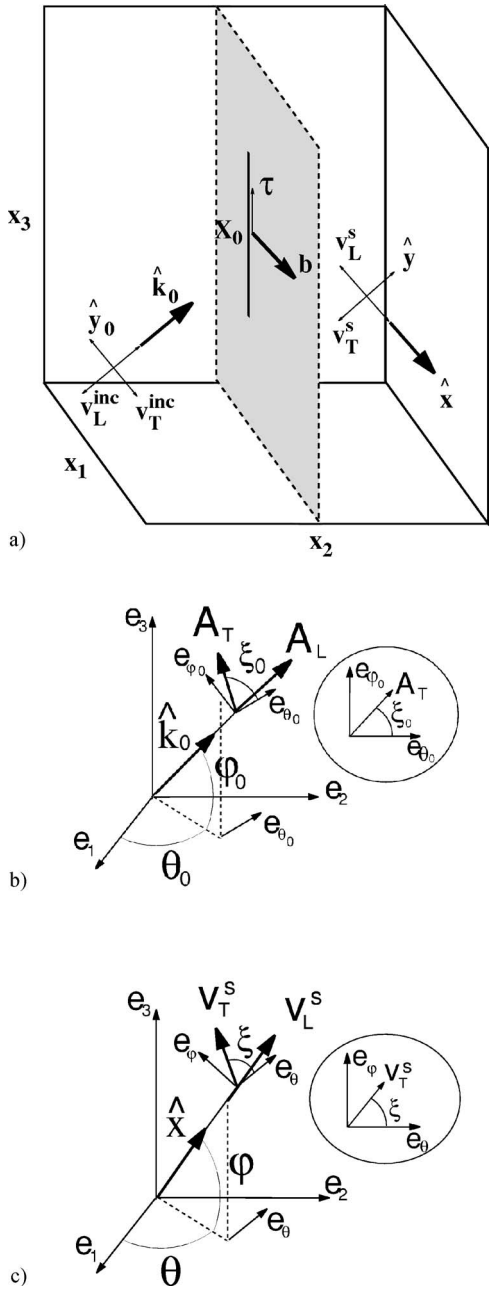

FIG. 3. (a) Convention chosen for the calculation of the scattering functions: the dislocation segment is along $\mathbf{e_3}$, the Burgers vector along $\mathbf{e_1}$. The incident wave propagates in the $\hat{\mathbf{k}}_0=\mathsf{R}_0\mathbf{e_1}$ direction and the scattering functions are calculated in the $\hat{\mathbf{x}}=\mathsf{R}\mathbf{e_1}$ direction with, in (b), (c), the definitions of the Euler angles $(\theta_0,\varphi_0,\xi_0)$ for R_0 and of the Euler angles (θ,φ,ξ) for R.

$$f_{TT}(\hat{\mathbf{x}}) = -\frac{2}{\pi^3}\left(\frac{\rho b^2}{m}\right) L\, S(\omega)\, f_T(\hat{\mathbf{k}}_0) g_T(\hat{\mathbf{x}}), \qquad (3.5)$$

with $g_L(\hat{\mathbf{x}}) \equiv {}^t\hat{\mathbf{x}}\mathsf{M}\hat{\mathbf{x}}$, $g_T(\hat{\mathbf{x}})\hat{\mathbf{y}} \equiv (\mathsf{I}-\hat{\mathbf{x}}{}^t\hat{\mathbf{x}})\mathsf{M}\hat{\mathbf{x}}$, $f_L(\hat{\mathbf{k}}_0) \equiv {}^t\hat{\mathbf{k}}_0\mathsf{M}\hat{\mathbf{k}}_0$ and $f_T(\hat{\mathbf{k}}_0) \equiv {}^t\hat{\mathbf{k}}_0\mathsf{M}\hat{\mathbf{y}}_0$. Note that the behavior for $\omega\to 0$ is given by $S(\omega)\to -1/\omega_1^2$ instead of the divergence that was obtained in two dimensional analysis.[13]

We choose the following conventions, illustrated in Fig. 3.

(i) The direction of the Burgers vector is along $\mathbf{e_1}(\mathbf{t}=\mathbf{e_1})$ and the direction of the dislocation line along $\mathbf{e_3}(\boldsymbol{\tau}=\mathbf{e_3})$.

(ii) The geometry of the incident wave with respect to the dislocation line is determined with Euler angles $(\theta_0,\varphi_0,\xi_0)$ and the corresponding rotation matrices $\mathsf{R}_0=\mathsf{R}(\mathbf{e_3},\theta_0)\mathsf{R}(\mathbf{e_2},\varphi_0)\mathsf{R}(\mathbf{e_1},\xi_0)$: $\hat{\mathbf{k}}_0=\mathsf{R}_0\mathbf{e_1}$ denotes the direction of the incident wave (thus also its direction of longitudinal polarization) and $\hat{\mathbf{y}}_0=\mathsf{R}_0\mathbf{e_2}$ denotes the direction of polarization of the incident transverse wave.

(iii) Similarly, the geometry of the scattered waves is determined using Euler angles (θ,φ,ξ) and the corresponding rotation matrices R: $\hat{\mathbf{x}}=\mathsf{R}\mathbf{e_1}$ denotes the direction of the scattered wave (thus also the direction of its longitudinal polarization) and $\hat{\mathbf{y}}=\mathsf{R}\mathbf{e_2}$ denotes the direction of polarization of the transverse scattered wave. Note that the direction of observation $\hat{\mathbf{x}}$ where the scattered wave is considered depends on (θ,φ) only. The third Euler angle ξ that gives the direction of polarization of the transverse scattered wave in the $(\mathbf{e}_\theta,\mathbf{e}_\varphi)$-plane must be determined. The explicit form of the rotation R is given in Eq. (A1).

This convention is not the usual one for the calculation of scattering amplitudes. Usually, the scattering direction $\hat{\mathbf{x}}$ is measured with respect to the direction of the incident wave. In our case, the forms of the scattering amplitudes are considerably simpler to manipulate with the chosen conventions. The scattering amplitudes take finally the form of Eqs. (3.5) with

$$f_L(\hat{\mathbf{k}}_0) = \cos^2\varphi_0 \sin 2\theta_0,$$

$$f_T(\hat{\mathbf{k}}_0) = \cos\varphi_0(\cos\xi_0\cos 2\theta_0 - \sin\varphi_0 \sin\xi_0 \sin 2\theta_0),$$

$$g_L(\hat{\mathbf{x}}) = \cos^2\varphi \sin 2\theta,$$

$$g_T(\hat{\mathbf{x}})\hat{\mathbf{y}} = \cos\varphi(\cos 2\theta\,\mathbf{e}_\theta - \sin\varphi \sin 2\theta\,\mathbf{e}_\varphi),$$

$$\text{or equivalently} \begin{cases} g_T(\hat{\mathbf{x}}) = -\cos\varphi\sqrt{1-\cos^2\varphi\sin^2 2\theta}, \\ \xi(\hat{\mathbf{x}}) = \tan^{-1}(\sin\varphi\tan 2\theta). \end{cases} \qquad (3.6)$$

Details of the calculation are given in Appendix A. Typical forms of the scattering functions are given in Fig. 4 for $\varphi_0=-\pi/5$, $\theta_0=\pi/4$, and $\xi_0=0$.

B. Interference patterns

In practice, the scattered wave superposes with the incident wave to produce an interference pattern, that it should be possible to see in numerical simulations as well as laboratory experiments. Experimentally, Shilo and Zolotoyabko[2–4] have developed a technique of stroboscopic x-ray imaging. By using a 580 MHz surface acoustic wave, they are able to visualize the interference pattern resulting from the interaction between acoustic waves and individual dislocations in $LiNbO_3$. Impressive contrast in a form of concentric rings can be seen in Refs. 2 and 3 for a dislocation line located perpendicularly to the crystal surface.

This experimental configuration differs from our theoretical one. For instance, because of the free surface, the waves

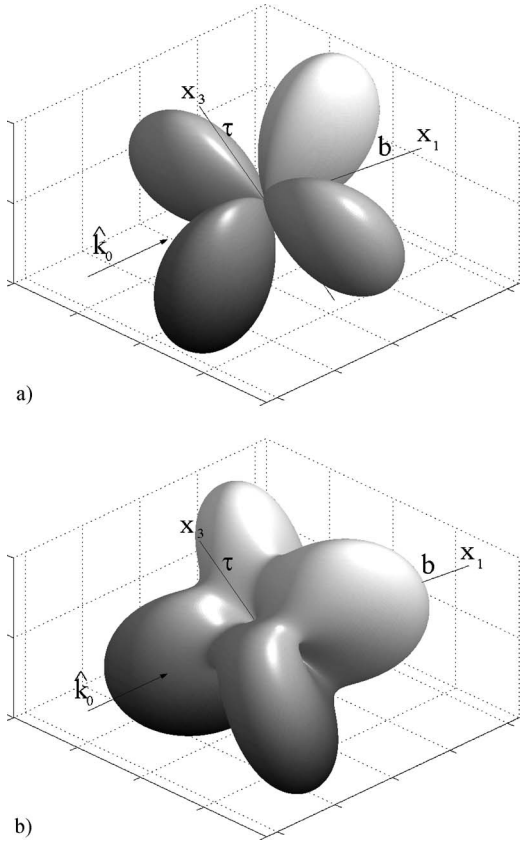

FIG. 4. Typical forms of the scattering amplitudes as a function of the direction $\hat{\mathbf{x}}$ (a) $f_{LL}(\hat{\mathbf{x}})$ and $f_{LT}(\hat{\mathbf{x}})$, having the same form given by $g_L(\hat{\mathbf{x}})$; (b) $f_{TL}(\hat{\mathbf{x}})$ and $f_{TT}(\hat{\mathbf{x}})$, having the same form given by $g_T(\hat{\mathbf{x}})$ for $\varphi_0=-\pi/5$, $\theta_0=\pi/4$, and $\xi_0=0$.

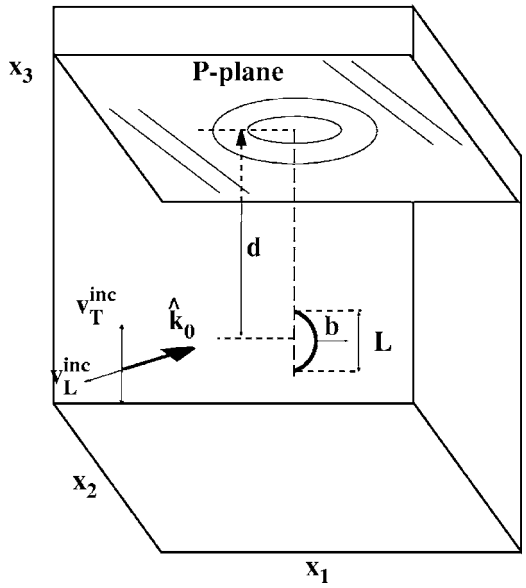

FIG. 5. A dislocation is located at a distance d from a free surface (here a P-plane) and its line is perpendicular to this plane (as in Fig. 1, dislocation bow out is exaggerated for the sake of clarity). The incident wave has both shear and longitudinal polarization; the shear polarization is perpendicular to the P-plane. The interference between the incident shear wave (along $\mathbf{e}_3$) and the $\mathbf{e}_3$-component of the scattered wave is observed in the P-plane.

excited in the experiment are surface waves, not bulk waves, and the elastic Green tensor for free space used in the present study should be replaced by the elastic Green tensor in a half-space for an accurate comparison. Also, wavelengths of a few μm are used in these experiments, so that our theoretical assumption $kL \ll 1$ will not hold for usual dislocation lengths. However, we can think that the physics of the interaction between the acoustic wave and the dislocation does not change significantly. Therefore, we suggest to study the configuration illustrated in Fig. 5 as an example to rationalize the trends and patterns observed in experimental visualizations. A dislocation segment, of length L is located at a distance d from the P-plane (the free surface) and is perpendicular to this plane. The incident wave propagates in the P-plane and hits the dislocation with an incident angle θ_0 with the Burgers vector. Finally, the wave has a longitudinal polarization and a transverse polarization perpendicular to the P-plane, as it is the case for surface waves. To calculate the interference pattern, it is then sufficient to (i) derive the scattered wave $\mathbf{v}^s(\mathbf{x})$ using the set of Eqs. (3.5) and (3.6) with $\varphi_0=0$, $\xi_0=\pi/2$, (ii) to extract the $v_3^s(\mathbf{x})$ component that is effectively measured by SAW technique, and finally (iii) to restrict the expression of $v_3^s(\mathbf{x})$ to $v_3^s(x_1,x_2)$, its expression in a plane $x_3=d$. With $[r=\sqrt{x_1^2+x_2^2}, \psi=\tan^{-1}(x_2/x_1)]$ the polar coordinates in the P-plane, we get

$$v_3^s(r,\psi) = -\frac{4}{\pi^3}\frac{\rho b^2}{m} S(\omega)\sin 2\theta_0 A_L(\gamma^{-3} e^{ik_L\sqrt{r^2+d^2}} - e^{ik_T\sqrt{r^2+d^2}}) \times \frac{d\, Lr^2 \cos\psi \sin\psi}{(d^2+r^2)^2}. \tag{3.7}$$

Note that only the longitudinal wave interacts with the dislocation for that incidence and generates both L and T waves due to mode conversion. Interference results from the superposition of the scattered wave v_3^s with the transverse incident wave

$$v(r,\psi) = v_3^s(r,\psi) + A_T e^{ik_T \cos(\theta_0-\psi)x} \tag{3.8}$$

in the P-plane. A typical form of the interference pattern is shown in Fig. 6(b) using $\omega=2\pi\,580$ MHz, $k_T=2\pi/6(\mu\text{m})^{-1}$, $d=10$ to 100 μm and arbitrary values of S and L (these two values give the weight of the scattered wave with respect to the incident one). Those theoretical patterns provide the pictures which could be compared qualitatively with those observed in Refs. 2,3. Figure 6(c) shows the modulation along a typical radius at constant ψ, a figure to be compared with Fig. 6 in Ref. 3, where a calculation is done assuming a constant scattering function. The aim of this calculation is to show that our approach can be helpful in the interpretation of these new experiments and that further theoretical developments along this direction (for instance the use of the appropriate Green function) will allow quantitative comparison.

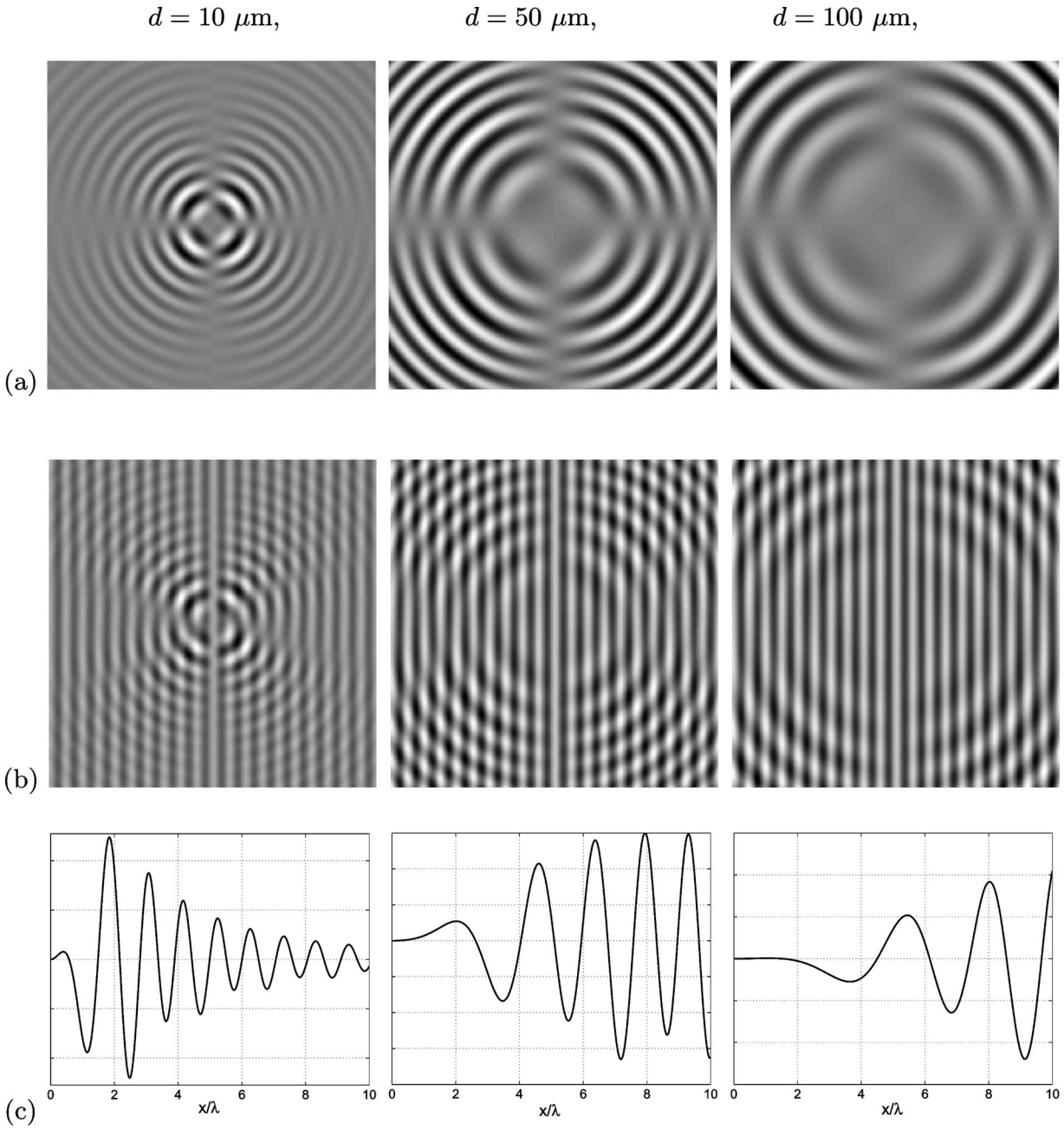

FIG. 6. From left to right, $d=10$, 50, and 100 μm, (a) $\mathbf{e}_3$ component of the scattered field in the P-plane, following Eq. (3.7). The horizontal axis coincides with the direction of the incident wave. (b) Resulting interference pattern [Eq. (3.8)]. (c) Typical modulation along a radius.

IV. THE OPTICAL THEOREM AND ENERGY LOSSES

A. The optical theorem for polarized waves

The time averaged total energy flux Π^a into a sphere containing the dislocation is $\Pi^a=\frac{1}{2}\mathrm{Re}\int \mathbf{dS}\ \sigma\mathbf{v}^*$. Decomposing the stress σ and velocity $\mathbf{v}$ into a sum of the incident part and scattered part $\sigma=\sigma^{\mathrm{inc}}+\sigma^s$, $\mathbf{v}=\mathbf{v}^{\mathrm{inc}}+\mathbf{v}^s$, leads to the definition of the scattered energy flux $\Pi^s=-\frac{1}{2}\mathrm{Re}\int \mathbf{dS}\ \sigma^s\mathbf{v}^{s*}$ and total energy flux, $\Pi^t=\Pi^a+\Pi^s$. Cross sections are usually defined normalizing the fluxes $\Pi^{a,s,t}$ with the incident flux $\Pi^{\mathrm{inc}}=\rho c_T(\gamma A_L^2+A_T^2)$. At leading order in $1/x$, the term $\sigma\mathbf{v}^*\ \mathbf{dS}$ reduces to

$$\rho\, x^2 d\Omega\left[c_L^2\frac{\partial u_r}{\partial x}v_r^* + c_T^2\left(\frac{\partial u_\theta}{\partial x}v_\theta^* + \frac{\partial u_\varphi}{\partial x}v_\varphi^*\right)\right],$$

where $d\Omega=\cos\varphi d\theta d\varphi$. It is shown in Appendix B that, for an incident wave of the form (3.3), the scattered and total energy fluxes are

$$\frac{d\Pi^s}{d\Omega}(\hat{\mathbf{x}}) = \frac{\rho c_T}{2}\{\gamma|f_{LL}(\hat{\mathbf{x}})A_L + f_{LT}(\hat{\mathbf{x}})A_T|^2 + |f_{TL}(\hat{\mathbf{x}})A_L + f_{TT}(\hat{\mathbf{x}})A_T|^2\},$$

$$\Pi^t = \frac{2\pi}{\omega}\rho c_T^2 \,\mathrm{Im}\{\gamma^2[f_{LL}(\hat{\mathbf{k}}_0)A_L + f_{LT}(\hat{\mathbf{k}}_0)A_T]A_L + c(\hat{\mathbf{k}}_0)[f_{TL}(\hat{\mathbf{k}}_0)A_L + f_{TT}(\hat{\mathbf{k}}_0)A_T]A_T\}, \tag{4.1}$$

where $c(\hat{\mathbf{k}}_0) \equiv {}^t\hat{\mathbf{y}}(\theta_0,\varphi_0)\hat{\mathbf{y}}_0 = \cos[\xi(\theta_0,\varphi_0) - \xi_0]$. This provides a relation between total energy flux and imaginary part of scattering amplitudes along the forward scattering direction usually known as an optical theorem. A more explicit form can be provided using Eqs. (3.5), in which case we find

$$\begin{aligned}\Pi^s &= \frac{16}{15\pi^5}\left(\frac{2}{\gamma^2} - 1\right)\left(\frac{\rho b^2}{m}\right)^2 \rho c_T L^2 |S(\omega)|^2 F(\mathbf{v}^{\mathrm{inc}}) \\ &\simeq \frac{16}{15\pi^5}\left(\frac{2}{\gamma^2} - 1\right)\left(\frac{\rho b^2}{m}\right)^2 \\ &\quad \times \rho c_T L^2 F(\mathbf{v}^{\mathrm{inc}}) \frac{\omega^4}{(\omega^2 - \omega_1^2)^2 + \omega^2 B^2/m^2}, \\ \Pi^t &= -\frac{4}{\pi^2}\rho c_T^2 L\left(\frac{\rho b^2}{m}\right)\mathrm{Im}\left(\frac{S(\omega)}{\omega}\right)F(\mathbf{v}^{\mathrm{inc}}) \\ &\simeq \frac{4}{\pi^2}\rho c_T^2 L\left(\frac{\rho b^2}{m}\right)F(\mathbf{v}^{\mathrm{inc}}) \frac{\omega^2 B/m}{(\omega^2 - \omega_1^2)^2 + \omega^2 B^2/m^2},\end{aligned} \tag{4.2}$$

where

$$F(\mathbf{v}^{\mathrm{inc}}) \equiv [\gamma^{-1} f_L(\hat{\mathbf{k}}_0)A_L + f_T(\hat{\mathbf{k}}_0)A_T]^2, \tag{4.3}$$

is a function that depends only on the characteristics of the incident wave (the incident direction $\hat{\mathbf{k}}_0$ and the amplitudes A_L and A_T). The scattering amplitudes f_L and f_T are given in Eqs. (3.6). The details of the calculation are given in Appendix B.

In our case, the scattering functions have been calculated in the first Born approximation. We can conclude that the absorption is given by the energy flux $\Pi^a \simeq \Pi^t$ at leading order but no conclusion is possible for higher order. Notably, when no internal viscosity exists ($B=0$), we get $\Pi^a \simeq 0$.

B. The energy loss per cycle

The energy loss per cycle ΔW is, at leading order,

$$\Delta W \equiv \frac{2\pi}{\omega}\Pi^t \simeq \frac{8}{\pi}\rho c_T^2 L\left(\frac{\rho b^2}{m}\right)F(\mathbf{v}^{\mathrm{inc}}) \frac{\omega B/m}{(\omega^2 - \omega_1^2)^2 + \omega^2 B^2/m^2} \tag{4.4}$$

with $F(\mathbf{v}^{\mathrm{inc}})$ defined in the preceding section in Eq. (4.3). Through this function F, the energy loss depends on the direction of the incident wave. This dependence is illustrated in Fig. 7.

For some directions of incidence the Peach-Koehler force vanishes, there is no interaction with the dislocation, and there is no energy loss. Specific cases are for an incident wave (either T or L) propagating along the dislocation line or for an incident L-wave propagating in a direction parallel or perpendicular to the Burgers vector $\mathbf{b}$ [Fig. 7(a)]. Also no interaction occurs for an incident T wave having a polarization along the dislocation line [Fig. 7(c)]. The opposite extreme is given by directions of maximum loss, corresponding to a maximum interaction. For instance, for a T-wave propagating along the direction of $\mathbf{b}$ with polarization perpendicu-

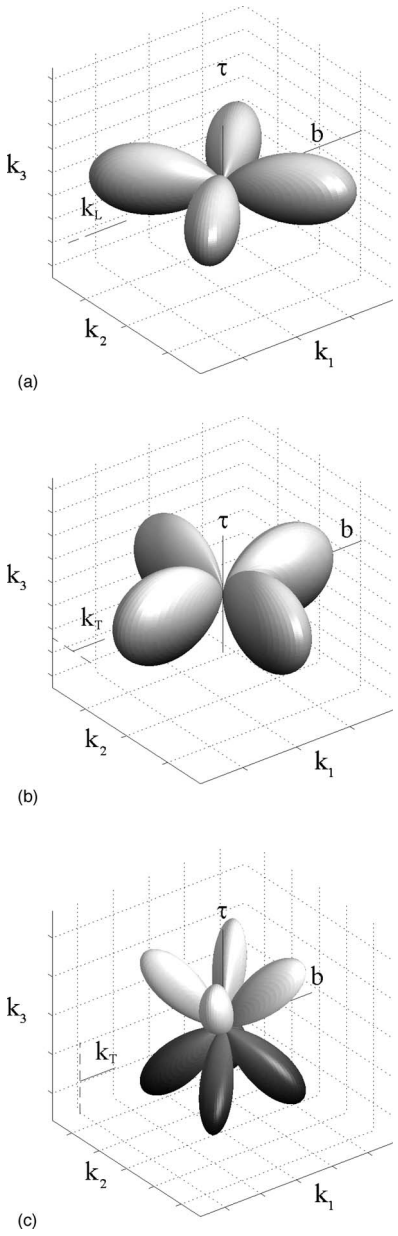

FIG. 7. Dependence $F(\mathbf{v}^{\mathrm{inc}})$ of the energy loss with the characteristic $\hat{\mathbf{k}}_0$ and $\hat{\mathbf{y}}_0$ of the incident wave. (a) Dependence on the direction of an incident L-wave ($A_T=0$) for which $F(\mathbf{v}^{\mathrm{inc}}) = f_L^2(\theta_0,\varphi_0)$. The dependence on the direction of the characteristics of an incident T-wave [$A_L=0$ for which $F(\mathbf{v}^{\mathrm{inc}}) = f_T^2(\theta,\varphi_0,\xi_0)$, with ξ_0 an extra variable] is represented for a polarization in the $(\mathbf{e}_{\theta_0},\mathbf{e}_{\varphi_0})$-plane (b) along $\mathbf{e}_{\theta_0}(\xi_0=0)$ or (c) along $\mathbf{e}_{\varphi_0}(\xi_0=\pi/2)$. For instance, for an incident T-wave propagating along the Burgers vector $\mathbf{e}_1$ for $\varphi_0=\theta_0=0$, (b) corresponds to a polarization along $\mathbf{e}_{\theta_0} = \mathbf{e}_2$ perpendicular to the slip plane, and (c) corresponds to a polarization along $\mathbf{e}_{\varphi_0} = \mathbf{e}_3$ parallel to the dislocation line. Vectors $k_{L,T}$ and the corresponding direction of polarization (in dotted lines) are represented for a particular incidence ($\theta_0=\varphi_0=0$) on each plot.

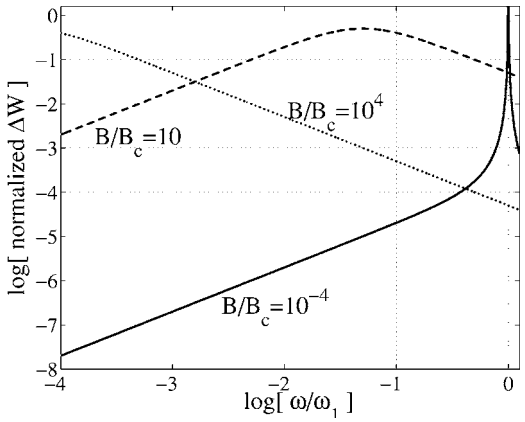

FIG. 8. Energy loss ΔW, normalized with $W_0 \sim (32/\pi^2) \times (\sigma_r^2/\mu) L^3$, as a function of the frequency $\omega[\omega_1 \simeq c_T \pi / L$ from Eq. (2.9)] for $B/B_c = 10^{-4}$ (underdamped regime), $B/B_c = 10, 10^4$ (overdamped regimes). $B_c = 2m\omega_1 \simeq 2\pi\Gamma/(c_T L)$ from Sec. II.

lar to the slip plane (in the direction of **n**) or propagating perpendicularly to the slip plane with a polarization parallel to **b** [Fig. 7(b)].

Another way to understand the function $F(\mathbf{v}^{\text{inc}})$ is to introduce the resolved stress σ_r that appears in the Peach-Koehler force when it is written in a scalar form $F = b\sigma_r$. In the chosen conventions, σ is the component $\sigma_{12}(\mathbf{X}_0 = \mathbf{0})$ of the stress tensor at the position of the dislocation. It is easy to see that the function $F(\mathbf{v}^{\text{inc}})$ is recovered in the strength of the resolved stress

$$\sigma_r = \rho c_T \left[\gamma^{-1} f_L(\hat{\mathbf{k}}_0) A_L + f_T(\hat{\mathbf{k}}_0) A_T \right]. \tag{4.5}$$

C. Energy loss versus frequency, comparison with a numerical experiment

We adopt in this section the following expression for the energy loss, using Eqs. (4.4) and (4.5):

$$\Delta W = \frac{8}{\pi} \left(\frac{\rho b^2}{m} \right) \frac{L}{\rho} \sigma_r^2 \frac{\omega B/m}{(\omega^2 - \omega_1^2)^2 + B^2 \omega^2 / m^2}. \tag{4.6}$$

The variation of ΔW with frequency, in the limit $\omega \ll \omega_1$, is straightforward. When ω becomes comparable to ω_1 several regimes must be distinguished. In the underdamped regime, ΔW is an increasing function of frequency up to the resonance frequency ω_1. In the overdamped regime, the energy loss reaches a maximum $\Delta W_{\max}$ at frequency $\omega_{\max}$,

$$\Delta W_{\max} = \frac{4}{\pi^3} \frac{b^2 L^3}{\Gamma} \sigma_r^2 \quad \text{for } \omega_{\max} = \pi^2 \frac{\Gamma}{BL^2} < \omega_1. \tag{4.7}$$

At frequencies low compared with $\omega_{\max}$, there is a linear increase with frequency, while at frequencies large compared to $\omega_{\max}$ it decreases as $1/\omega$. It follows also that an increase in Γ increases the energy loss and shifts the peak to higher frequencies while an increase in B simply shifts the peak to lower frequencies, a natural trend for a damped linear oscillator.

These behaviors are illustrated in Fig. 8 where the energy loss has been normalized with $W_0 = 8/\pi (\rho b^2/m) L \sigma_r^2 / (\rho \omega_1^2) \simeq (32/\pi^2)(\sigma_r^2/\mu) L^3$. Incidentally, note that the energy W_0 differs from the incident energy defined in Refs. 14 and 25. Using dimensional arguments, it is possible to define the incident energy in a volume L^3 as $W^{\text{inc}} = \Pi^{\text{inc}} L^3 / c_T$, with $\Pi^{\text{inc}} = \rho c_T (\gamma A_L^2 + A_T^2)$ but no general relation exists between σ_r and Π^{inc}. As previously seen, this is because the efficiency of the interaction with the dislocation depends on the direction of the polarizations of the incident wave. Thus, whatever the strength of incident energy W^{inc}, ineffective directions make W^0 vanish.

We consider now a configuration numerically studied in Refs. 5 and 6. Those calculations are based on a continuum simulation of dislocation dynamics, when each segment of the dislocation line between the two endpoints verifies an equation of motion similar to our Eq. (2.1) where the inertial term is neglected and where the line tension is taken into account through the so-called self-stress.[29,30] The energy loss is defined as

$$\Delta W = \left\langle \int_t^{t+2\pi/\omega} dt \; \sigma_r b \cos \omega t \frac{\partial A}{\partial t} dt \right\rangle, \tag{4.8}$$

where $A(t) \equiv \int_{\mathcal{L}} ds \; X(s,t)$ denotes the area swept by the dislocation line, σ_r denotes the resolved stress, and angular brackets denote the average over several cycles because the numerical time evolution is not perfectly periodic. It is shown in Appendix C that this definition is equivalent to our definition in Eq. (4.6), with

$$A(t) = -\frac{8}{\pi^2} \frac{bL}{m} \sigma_r \left(\frac{(\omega^2 - \omega_1^2)\cos \omega t - \omega B/m \sin \omega t}{(\omega^2 - \omega_1^2)^2 + \omega^2 B^2 / m^2} \right), \tag{4.9}$$

when $\sigma_r(t) = \sigma_r \cos \omega t$.

To make more precise the independence of ΔW with respect to the mass in the overdamped regime, note that Eq. (4.6) can also be written, using Eq. (2.9),

$$\Delta W = \frac{8}{\pi} b^2 L \sigma_r^2 \frac{\omega B}{\left[m\omega^2 - \Gamma \left(\frac{\pi}{L} \right)^2 \right]^2 + \omega^2 B^2}, \tag{4.10}$$

and the term in $m\omega^2$ can be neglected for overdamped regime $B \gg B_c$ and $\omega \ll \omega_1$. In our model, a precise value of Γ in Eq. (2.3) needs the ratio of the long- over small-cutoff lengths to be known (usually, $\delta \sim L$ and $\delta_0 \sim b$). Taking $\ln(\delta/\delta_0)$ of order one, we can calculate the curve $\Delta W(\omega)$ in the same conditions as described in Refs. 5 and 6 and without any additional adjustable parameter, a $L = 1$ μm dislocation line is driven by a $\sigma_r = 0.5$ MPa sinusoidal stress in the range $10^3 - 10^7$ Hz. The other constants are $b = 2.86$ A, $\mu = 26.5$ GPa, $\nu = 0.347$ [with ν the Poisson's ratio, so that $\gamma = \sqrt{2(1-\nu)/(1-2\nu)}$] $B = 0.08$ Pa s, and we take $\rho = 2300$ kg/m^3 for aluminum. Figure 9 shows the curve obtained in comparison with numerical results of Ref. 6. The results reasonably compare. The values of $\omega_{\max}$ are in good agreement but the energy maximum is a factor about 2.5 higher in numerical experiments. This discrepancy is not due to a difference in the line tension value because in that case

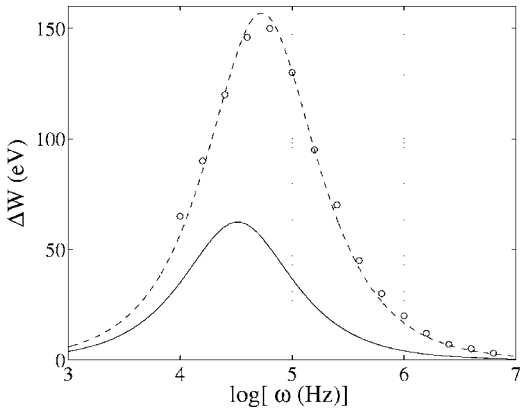

FIG. 9. Energy loss calculated from Eq. (4.6) in solid line with values taken from Ref. 6, circles (with dashed line) indicate the values obtained from the corresponding numerical experiments (from Fig. 3 in Ref. 6).

$\omega_{\max}$ would be different as well. Further work is needed to understand this discrepancy.

Note also that the calculations of Greaney *et al.* do not include radiation. However, direct comparison with our calculation remains possible at first order. Indeed, at this first order, the equation for the motion of the dislocation in Eq. (2.1) has the form of the equation of motion for a string forced by an harmonic stress ($v=v^{\text{inc}}$ in the Peach-Koehler force), as considered in Ref. 6.

V. CONCLUDING REMARKS

The scattering by a dislocation segment has been investigated in the low frequency regime with respect to the natural oscillation frequency of the dislocation ($kL \ll 1$). Conventional experiments, being performed in the kHz to MHz regime, involve wavelengths ranging from a few meters to a few millimeters, well above typical micrometer length of dislocations. However, care should be taken when applying the theory to explain recent experiments reaching the GHz frequency regime.

Also, calculations have been performed considering a gliding edge dislocation. Many real materials involve mixed dislocations whose Burgers vector is the sum of edge and screw dislocation Burgers vectors. Since all phenomena discussed in this study are linear, the case of mixed dislocations can be obtained by superposition. Also, since continuum elasticity is considered, there is no restriction on the value of the Burgers vector which does not need to be a lattice vector and our results apply without change to partials.

The interaction of an elastic wave with a single dislocation has been characterized by the scattering functions and it has been shown that the strength of the interaction depends on the frequency and on the characteristics of the incident wave. This is a step forward which, we expect, will allow us to enable a quantitative comparison between theory and modern experiments[2–4] and, on this basis, the extraction with high precision of important parameters such as dislocation viscosity. Our scattering formalism, that takes into full account the vector nature of the elastic wave dislocation interaction, can deal with these new situations that involve free surfaces and short wavelengths ($kL \gg 1$) such as are used in SAW experiments.[2–4]

Finally, a natural extension of the present study is to consider a random distribution of dislocations to account for collective behavior, a study that is presented in Ref. 1.

ACKNOWLEDGMENTS

This work has been supported by ECOS Grant No. C04E01 and by FONDAP Grant No. 11980002. One of the authors (F.B.) thanks Fondecyt project 1030556. Two of the authors (A.M. and V.P.) are pleased to thank Erik Bitzek for fruitful discussions.

APPENDIX A: TECHNICAL CALCULATIONS ON THE SCATTERING FUNCTIONS

We define the rotation matrix $\mathsf{R} \equiv \mathsf{R}(\mathbf{e_3}, \theta)\mathsf{R}(\mathbf{e_2}, \varphi)\mathsf{R}(\mathbf{e_1}, \xi)$,

$$\mathsf{R} = \begin{pmatrix} \cos\varphi\cos\theta & -\sin\theta\cos\xi - \sin\varphi\cos\theta\sin\xi & \sin\theta\sin\xi - \sin\varphi\cos\theta\cos\xi \\ \cos\varphi\sin\theta & \cos\theta\cos\xi - \sin\varphi\sin\theta\sin\xi & -\cos\theta\sin\xi - \sin\varphi\sin\theta\cos\xi \\ \sin\varphi & \cos\varphi\sin\xi & \cos\varphi\cos\xi \end{pmatrix} \tag{A1}$$

defined with the Euler angles (θ, φ, ξ) is the matrix from $(\mathbf{e_1}, \mathbf{e_2}, \mathbf{e_3})$ to $(\mathbf{e_r}, \mathbf{e}_\xi, \mathbf{e_r} \times \mathbf{e}_\xi)$, as illustrated in Fig. 10.

The scattering functions are defined in Eqs. (3.5) with $g_L(\hat{\mathbf{x}}) \equiv {}^t\hat{\mathbf{x}}\mathsf{M}\hat{\mathbf{x}}$, $g_T(\hat{\mathbf{x}})\hat{\mathbf{y}} \equiv (\mathsf{I} - \hat{\mathbf{x}}{}^t\hat{\mathbf{x}})\mathsf{M}\hat{\mathbf{x}}$, $f_L(\hat{\mathbf{k}}_0) \equiv {}^t\hat{\mathbf{k}}_0\mathsf{M}\hat{\mathbf{k}}_0$ and $f_T(\hat{\mathbf{k}}_0) \equiv {}^t\hat{\mathbf{k}}_0\mathsf{M}\hat{\mathbf{y}}_0$. Without loss of generality, we choose $\mathbf{b} = b\mathbf{e_1}$, $\mathbf{n} = \mathbf{e_2}$ and $\boldsymbol{\tau} = \mathbf{e_3}$, so that M takes a simple form

$$\mathsf{M} = \mathbf{e_1}{}^t\mathbf{e_2} + \mathbf{e_2}{}^t\mathbf{e_1}. \tag{A2}$$

The polarizations $\mathbf{A_L}$ and $\mathbf{A_T}$ of the incident wave can have any direction with respect to the dislocation segment so that we note $\mathbf{A}_L = A_L\mathsf{R}_0\mathbf{e_1}$ and $\mathbf{A}_T = A_T\mathsf{R}_0\mathbf{e_2}$, where R_0 is the rotation matrix of Euler angles $(\theta_0, \varphi_0, \xi_0)$ (the corresponding configuration is illustrated in Fig. 3). This means also that the

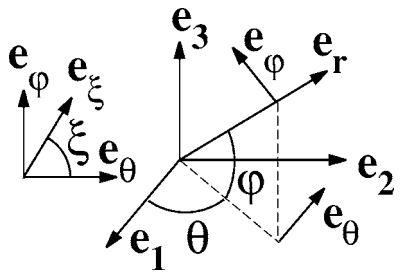

FIG. 10. Euler angles.

incident wave propagates along the direction of vector $\mathsf{R}^0\hat{\mathbf{e}}_1$.

Similarly, we define the direction of observation $\hat{\mathbf{x}}=\mathsf{R}\mathbf{e}_1$ [this direction depends only on (θ,φ) in spherical coordinates]. The polarizations of the scattered waves are denoted $\mathbf{A}_L=A_L\mathsf{R}\mathbf{e}_1$ (along the direction of observation) and $\mathbf{A}_T=A_T\mathsf{R}\mathbf{e}_2$. The direction of the shear wave $\mathbf{y}$ has one more degree of freedom ξ than the compressional wave, this angle being *a priori* a function of the geometry of the dislocation segment and of the direction of observation. It will be shown below that the direction of polarization of the shear wave depends only on the direction of observation, that is $\xi=\xi(\theta,\varphi)$.

The derivation of the functions f is below, with $\hat{\mathbf{k}}_0=[\cos\varphi_0\cos\theta_0;\cos\varphi_0\sin\theta_0;\sin\varphi_0]$

$$f_L(\hat{\mathbf{k}}_0)\equiv {}^t\hat{\mathbf{k}}_0\mathsf{M}\hat{\mathbf{k}}_0=2\mathsf{R}_{0,11}\mathsf{R}_{0,21}=\cos^2\varphi_0\sin 2\theta_0,$$

$$\begin{aligned}f_T(\hat{\mathbf{k}}_0)&\equiv {}^t\hat{\mathbf{k}}_0\mathsf{M}\hat{\mathbf{y}}_0=\mathsf{R}_{0,11}\mathsf{R}_{0,22}+\mathsf{R}_{0,21}\mathsf{R}_{0,12}\\&=\cos\varphi_0[\cos\xi_0\cos 2\theta_0-\sin\varphi_0\sin\xi_0\sin 2\theta_0]\end{aligned}\tag{A3}$$

g_L is easily obtained, with $\hat{\mathbf{x}}=[\cos\varphi\cos\theta;\cos\varphi\sin\theta;\sin\varphi]$

$$g_L(\hat{\mathbf{x}})\equiv {}^t\hat{\mathbf{x}}\mathsf{M}\hat{\mathbf{x}}=2\mathsf{R}_{11}\mathsf{R}_{21}=\cos^2\varphi\sin 2\theta.\tag{A4}$$

To get $g_T\hat{\mathbf{y}}$, we find its components along $\mathbf{e}_\theta$ and $\mathbf{e}_\varphi$,

$$\begin{aligned}g_T(\hat{\mathbf{x}})\cos\xi&={}^t\mathbf{e}_\theta(\mathsf{I}-\hat{\mathbf{x}}{}^t\hat{\mathbf{x}})\mathsf{M}\hat{\mathbf{x}}={}^t\mathbf{e}_\theta(\mathbf{e_1}{}^t\mathbf{e_2}+\mathbf{e_2}{}^t\mathbf{e_1})\hat{\mathbf{x}}-g_L{}^t\mathbf{e}_\theta\hat{\mathbf{x}}\\&=e_{\theta,1}\hat{x}_2+e_{\theta,2}\hat{x}_1=\cos\varphi\cos 2\theta\end{aligned}$$

$$\begin{aligned}g_T(\hat{\mathbf{x}})\sin\xi&={}^t\mathbf{e}_\varphi(\mathsf{I}-\hat{\mathbf{x}}{}^t\hat{\mathbf{x}})\mathsf{M}\hat{\mathbf{x}}={}^t\mathbf{e}_\varphi(\mathbf{e_1}{}^t\mathbf{e_2}+\mathbf{e_2}{}^t\mathbf{e_1})\hat{\mathbf{x}}-g_L{}^t\mathbf{e}_\varphi\hat{\mathbf{x}}\\&=e_{\varphi,1}\hat{x}_2+e_{\varphi,2}\hat{x}_1=-\cos\varphi\sin\varphi\sin 2\theta\end{aligned}\tag{A5}$$

that can be written as

$$g_T(\hat{\mathbf{x}})\hat{\mathbf{y}}=\cos\varphi(\cos 2\theta\mathbf{e}_\theta-\sin\varphi\sin 2\theta\mathbf{e}_\varphi),\tag{A6}$$

or

$$\begin{aligned}g_T(\hat{\mathbf{x}})&=-\cos\varphi\sqrt{1-\cos^2\varphi\sin^2 2\theta},\\\xi(\hat{\mathbf{x}})&=\tan^{-1}(\sin\varphi\tan 2\theta).\end{aligned}\tag{A7}$$

APPENDIX B: TECHNICAL CALCULATIONS FOR THE DERIVATION OF THE SCATTERING AND TOTAL CROSS SECTIONS

1. On the scattered cross section

The scattered energy flux is defined by $\Pi^s=-\frac{1}{2}\mathrm{Re}\int d\mathbf{S}\ \sigma^s\mathbf{v}^{s*}$, where $d\mathbf{S}=x^2d\Omega\hat{\mathbf{x}}$ ($d\Omega$ is the solid angle).

We choose spherical coordinates, where $v_r^s=v_L^s$, $v_\theta^s=v_T^s\,{}^t\hat{\mathbf{y}}\mathbf{e}_\theta$ and $v_\varphi^s=v_T^s\,{}^t\hat{\mathbf{y}}\mathbf{e}_\varphi$. The stress tensor is written at leading order in $1/x$, $\sigma_{rr}\simeq\rho c_L^2\partial u_r/\partial x$, $\sigma_{r\theta}\simeq\rho c_T^2\partial u_\theta/\partial x$ and $\sigma_{r\varphi}\simeq\rho c_T^2\partial u_\varphi/\partial x$. We thus get

$$\begin{aligned}\Pi^s&=-\frac{\rho}{2}\mathrm{Re}\int dS\left[c_L^2\frac{\partial u_r^s}{\partial x}v_r^{s*}+c_T^2\left(\frac{\partial u_\theta^s}{\partial x}v_\theta^{s*}+\frac{\partial u_\varphi^s}{\partial x}v_\varphi^{s*}\right)\right]\\&=\frac{\rho}{2}\mathrm{Re}\int dS[c_L|v_r^s|^2+c_T(|v_\theta^s|^2+|v_\varphi^s|^2)],\end{aligned}\tag{B1}$$

where we have used that $\partial u_a/\partial x=-v_a/a$, $a=c_L$, c_T. We thus get, using the general definition of the scattering amplitudes in Eqs. (3.5),

$$\Pi^s=\frac{\rho}{2}\int d\Omega[c_L|f_{LL}A_L+f_{LT}A_T|^2+c_T|f_{TL}A_L+f_{TT}A_T|^2],\tag{B2}$$

that is the first relation of Eq. (4.1)

Let us use now our particular expression of the scattering amplitudes in Eqs. (3.5),

$$\begin{aligned}\Pi^s=\frac{4}{\pi^6}\left(\frac{\rho b^2}{m}\right)^2L^2|S(\omega)|^2\frac{\rho}{2}c_T\int d\Omega[(\gamma^{-2}g_L^2+g_T^2)\\\times(\gamma^{-1}f_LA_L+f_TA_T)^2].\end{aligned}\tag{B3}$$

The function $(\gamma^{-1}f_LA_L+f_TA_T)^2$ depends only on the characteristic of the incident wave. The integration over $d\Omega=\cos\varphi d\varphi d\theta$ is performed using Eqs. (3.6) for $\gamma^{-2}g_L^2+g_T^2=(\gamma^{-2}-1)\cos^4\varphi\sin^2 2\theta-\cos^2\varphi$, leading to $\int d\Omega(\gamma^{-2}g_L^2+g_T^2)=8\pi(2\gamma^{-2}-1)/15$ and

$$\Pi^s=\frac{16}{15\pi^5}(2\gamma^{-2}-1)\rho c_T\left(\frac{\rho b^2}{m}\right)^2L^2|S(\omega)|^2F(\mathbf{v}^{\mathrm{inc}}),\tag{B4}$$

where

$$F(\mathbf{v}^{\mathrm{inc}})\equiv[\gamma^{-1}f_L(\hat{\mathbf{k}}_0)A_L+f_T(\hat{\mathbf{k}}_0)A_T]^2,\tag{B5}$$

with f_L, f_T given by Eqs. (3.6). This equation is the first relation of Eqs. (4.2).

2. On the total cross section

The total energy flux is defined by $\Pi^t=\frac{1}{2}\mathrm{Re}\int d\mathbf{S}(\sigma^s\mathbf{v}^{\mathrm{inc}*}+\sigma^{\mathrm{inc}}\mathbf{v}^{s*})$. With the same notations as in the preceding section, we easily get that $\sigma^s\mathbf{v}^{\mathrm{inc}}=-\rho c_T(\gamma v_L^s\,{}^t\hat{\mathbf{x}}+v_T^s\,{}^t\hat{\mathbf{y}})(v_L^{\mathrm{inc}}\hat{\mathbf{k}}_0+v_T^{\mathrm{inc}}\hat{\mathbf{y}}_0)^*$ and $\sigma^{\mathrm{inc}}\mathbf{v}^s=[\sigma^s\mathbf{v}^{\mathrm{inc}}]^*\,{}^t\hat{\mathbf{k}}_0\hat{\mathbf{x}}$. We thus have

$$\begin{aligned}\int d\mathbf{S}\ \sigma^s\mathbf{v}^{\mathrm{inc}*}=-\frac{\rho c_T}{2}\int x^2d\Omega(\gamma v_L^s\,{}^t\hat{\mathbf{x}}+v_T^s\,{}^t\hat{\mathbf{y}})\\\times(v_L^{\mathrm{inc}}\hat{\mathbf{k}}_0+v_T^{\mathrm{inc}}\hat{\mathbf{y}}_0)^*,\end{aligned}$$

$$\int d\mathbf{S}\ \sigma^{\mathrm{inc}}\mathbf{v}^{s*} = -\frac{\rho c_T}{2}\int x^2 d\Omega(\gamma v_L^s\ {}^t\hat{\mathbf{x}} + v_T^s\ {}^t\hat{\mathbf{y}})^* \times (v_L^{\mathrm{inc}}\hat{\mathbf{k}}_0 + v_T^{\mathrm{inc}}\hat{\mathbf{y}}_0)\ {}^t\hat{\mathbf{k}}_0\hat{\mathbf{x}}. \tag{B6}$$

Let us calculate the first of the integrals in the above Eqs. (B6). The terms in $v_L^{\mathrm{inc}*}$, $v_T^{\mathrm{inc}*}$ introduce a term in $e^{-ik\ {}^t\hat{\mathbf{k}}_0\hat{\mathbf{x}}} = e^{-ikxG(\theta,\varphi)}$, $k=k_L,k_T$ [namely $G(\theta,\varphi)=\cos\varphi\cos\varphi_0\cos(\theta-\theta_0)+\sin\varphi\sin\varphi_0$]. It is now convenient to define the generic integral

$$I(g,k) \equiv \int x\cos\varphi d\varphi d\theta\ g(\theta,\varphi)e^{-ikxG(\theta,\varphi)} = \frac{2i\pi}{k}g(\theta_0,\varphi_0)e^{-ikx}, \tag{B7}$$

where we have used twice a stationary phase approximation, valid at large distances from the dislocation, $kx\gg 1$, with φ and θ. We get

$$\begin{aligned}\int d\mathbf{S}\ \sigma^s\mathbf{v}^{\mathrm{inc}*} = -\frac{\rho c_T}{2}\{&e^{ik_Lx}I[\gamma(f_{LL}A_L+f_{LT}A_T)A_L\ {}^t\hat{\mathbf{x}}\hat{\mathbf{k}}_0,k_L]\\ &+e^{ik_Tx}I[\gamma(f_{TL}A_L+f_{TT}A_T)A_L\ {}^t\hat{\mathbf{y}}\hat{\mathbf{k}}_0,k_L]\\ &+e^{ik_Lx}I[\gamma(f_{LL}A_L+f_{LT}A_T)A_T\ {}^t\hat{\mathbf{x}}\hat{\mathbf{y}}_0,k_T]\\ &+e^{ik_Tx}I[(f_{TL}A_L+f_{TT}A_T)A_T\ {}^t\hat{\mathbf{y}}\hat{\mathbf{y}}_0,k_T]\hat{\mathbf{x}}\}\\ =-\rho c_T i\pi\Big(&\gamma[f_{LL}(\hat{\mathbf{k}}_0)A_L+f_{LT}(\hat{\mathbf{k}}_0)A_T]\frac{A_L}{k_L}\\ &+[f_{TL}(\hat{\mathbf{k}}_0)A_L+f_{TT}(\hat{\mathbf{k}}_0)A_T]\frac{A_T}{k_T}c(\hat{\mathbf{y}}_0)\Big).\end{aligned} \tag{B8}$$

We have used that $\mathbf{x}$ equals $\hat{\mathbf{k}}_0$ in the forward direction $\theta=\theta_0$, $\varphi=\varphi_0$, and that ${}^t\hat{\mathbf{y}}(\theta_0,\varphi_0)\hat{\mathbf{k}}_0={}^t\hat{\mathbf{x}}(\theta_0,\varphi_0)\hat{\mathbf{y}}_0=0$ (this implies that the coupling between A_L and A_T vanishes). However, $\hat{\mathbf{y}}(\theta_0,\varphi_0)$ differs in general from $\hat{\mathbf{y}}_0$ and we denote $c(\hat{\mathbf{k}}_0)\equiv{}^t\hat{\mathbf{y}}(\theta_0,\varphi_0)\hat{\mathbf{y}}_0=\cos[\xi(\theta_0,\varphi_0)-\xi_0]$. The same procedure applied to the second integral in Eqs. (B6) gives

$$\int d\mathbf{S}\ \sigma^{\mathrm{inc}}\mathbf{v}^{s*} = \rho c_T i\pi\Big(\gamma[f_{LL}(\hat{\mathbf{k}}_0)A_L+f_{LT}(\hat{\mathbf{k}}_0)A_T]\frac{A_L}{k_L} +[f_{TL}(\hat{\mathbf{k}}_0)A_L+f_{TT}(\hat{\mathbf{k}}_0)A_T]\frac{A_T}{k_T}c(\hat{\mathbf{y}}_0)\Big)^*. \tag{B9}$$

Coming back to Π^t, we finally get

$$\Pi^t = 2\pi\rho c_T\,\mathrm{Im}\Big(\gamma[f_{LL}(\hat{\mathbf{k}}_0)A_L+f_{LT}(\hat{\mathbf{k}}_0)A_T]\frac{A_L}{k_L} +[f_{TL}(\hat{\mathbf{k}}_0)A_L+f_{TT}(\hat{\mathbf{k}}_0)A_T]c(\hat{\mathbf{y}}_0)\frac{A_T}{k_T}\Big), \tag{B10}$$

that is equivalently written in the form of the second relation in Eqs. (4.1).

Again, we develop the previous relation in our particular case. Using Eqs. (3.5), we get

$$\Pi^t = -\frac{4}{\pi^2}\rho c_T^2 L\Big(\frac{\rho b^2}{m}\Big)\mathrm{Im}\Big(\frac{S(\omega)}{\omega}\Big)[\gamma^{-1}f_L(\hat{\mathbf{k}}_0)A_L+f_T(\hat{\mathbf{k}}_0)A_T] \times[\gamma^{-1}g_L(\hat{\mathbf{k}}_0)A_L+g_T(\hat{\mathbf{k}}_0)c(\hat{\mathbf{y}}_0)A_T]. \tag{B11}$$

Using Eqs. (3.6), it is easy to see that $g_T(\hat{\mathbf{k}}_0)c(\hat{\mathbf{y}}_0) = g_T(\hat{\mathbf{k}}_0)\,{}^t\hat{\mathbf{y}}_0\hat{\mathbf{y}}=f_T(\hat{\mathbf{k}}_0)$, from which we finally have

$$\Pi^t = -\frac{4}{\pi^2}\rho c_T^2 L\Big(\frac{\rho b^2}{m}\Big)\mathrm{Im}\Big(\frac{S(\omega)}{\omega}\Big)F(\mathbf{v}^{\mathrm{inc}}), \tag{B12}$$

with $F(\mathbf{v}^{\mathrm{inc}})$ is defined in Eq. (B5). This equation is the second relation of Eqs. (4.2).

APPENDIX C: ON ENERGY LOSSES

The energy loss is often defined as the work done by the Peach-Koehler force to displace the dislocation

$$\Delta W = \int_t^{t+2\pi/\omega} dt\int_{\mathcal{L}} ds\ F(s,t)\frac{\partial X}{\partial t}(s,t). \tag{C1}$$

For a sinusoidal resolved stress $\sigma_r(\mathbf{X}_0,t)=\sigma_r\cos\omega t$, all quantities are written as $Y(x,t)=\mathrm{Re}[Y(x,\omega)e^{-i\omega t}]$. Defining $A(t)=\int_{\mathcal{L}}ds\ X(s,t)$ the area swept by the dislocation line and assuming the force $F(s,t)$ equal $F(\mathbf{X}_0,t)=\sigma_r b\cos\omega t$ (this is the approximation $kL\ll 1$), we get

$$\Delta W = \int_t^{t+2\pi/\omega} dt\ \sigma_r b\cos\omega t\frac{\partial A}{\partial t}. \tag{C2}$$

This Eq. (C2) is the expression used in the numerical experiments of Ref. 5,6. The area swept by the dislocation line is deduced from Eq. (2.7) using that $\mu\mathsf{M}_{lk}\partial_l v_k(\mathbf{X}_0,\omega)=-i\omega\sigma_r$ and Eq. (3.1),

$$\begin{aligned}A(t) &= -\frac{8}{\pi^2}\frac{bL}{m}\sigma_r\,\mathrm{Re}\Big(\frac{e^{-i\omega t}}{\omega^2-\omega_1^2+i\omega B/m}\Big)\\ &= -\frac{8}{\pi^2}\frac{bL}{m}\sigma_r\Big(\frac{(\omega^2-\omega_1^2)\cos\omega t-\omega B/m\sin\omega t}{(\omega^2-\omega_1^2)^2+\omega^2B^2/m^2}\Big).\end{aligned} \tag{C3}$$

We finally obtain

$$\begin{aligned}\Delta W &= \frac{8}{\pi^2}\frac{b^2L}{m}\sigma_r^2\int_t^{t+2\pi/\omega}dt\frac{\omega^2B/m}{(\omega^2-\omega_1^2)^2+\omega^2B^2/m^2}\cos^2\omega t\\ &= \frac{8}{\pi}\frac{b^2L}{m}\sigma_r^2\frac{\omega B/m}{(\omega^2-\omega_1^2)^2+\omega^2B^2/m^2}.\end{aligned} \tag{C4}$$

Equation (C4) corresponds to our expression of the energy loss given in Eq. (4.6).

[1] A. Maurel, V. Pagneux, F. Barra, and F. Lund, following paper, Phys. Rev. B **72**, 174111 (2005).
[2] E. Zolotoyabko, D. Shilo, and E. Lakin, Mater. Sci. Eng., A **309-310**, 23 (2001).
[3] D. Shilo and E. Zolotoyabko, Ultrasonics **40**, 921 (2002).
[4] D. Shilo and E. Zolotoyabko, Phys. Rev. Lett. **91**, 115506 (2003).
[5] P. A. Greaney and D. C. Chrzan, Mater. Res. Soc. Symp. Proc. **578**, 161 (1999).
[6] P. A. Greaney, L. H. Friedman, and D. C. Chrzan, Comput. Mater. Sci. **25**, 387 (2002).
[7] F. R. N. Nabarro, Proc. R. Soc. London, Ser. A **209**, 278 (1951).
[8] J. D. Eshelby, Proc. R. Soc. London, Ser. A **197**, 396 (1949).
[9] J. D. Eshelby, Phys. Rev. **90**, 248 (1953).
[10] T. Mura, Philos. Mag. **8**, 843 (1963).
[11] J. Kiusalaas and T. Mura, Philos. Mag. **9**, 1 (1963).
[12] F. Lund, J. Mater. Res. **3**, 280 (1988).
[13] A. Maurel, J.-F. Mercier, and F. Lund, J. Acoust. Soc. Am. **115**, 2773 (2004).
[14] A. V. Granato and K. Lücke, in *Physical Acoustics*, edited by W. P. Mason (Academic, New York, 1966), Vol 4A.
[15] A. V. Granato and K. Lücke, J. Appl. Phys. **27**, 583 (1956).
[16] A. V. Granato and K. Lücke, J. Appl. Phys. **27**, 789 (1956).
[17] K. Lücke and A. V. Granato, Phys. Rev. B **24**, 6991 (1981).
[18] G. A. Kneezel and A. V. Granato, Phys. Rev. B **25**, 2851 (1982).
[19] A. Maurel, J.-F. Mercier, and F. Lund, Phys. Rev. B **70**, 024303 (2004).
[20] F. C. Frank and W. T. Read, Jr., Phys. Rev. **79**, 722 (1950).
[21] E. M. Nadgornyi, Prog. Mater. Sci. **31**, 1 (1988).
[22] N. F. Mott, Philos. Mag. **43**, 1151 (1952).
[23] J. Friedel, Philos. Mag. **44**, 444 (1953).
[24] M. O. Peach and J. S. Koehler, Phys. Rev. **80**, 436 (1950).
[25] J. S. Koehler, in *Imperfections in Nearly Perfect Crystals*, edited by W. Schockley *et al.* (Wiley, New York, 1952).
[26] M. Hiratani and E. M. Nadgornyi, Acta Mater. **49**, 4337 (2001).
[27] J. Weertman, J. Appl. Phys. **26**, 202 (1954).
[28] A. E. H. Love, *The Mathematical Theory of Elasticity* (Dover, New York, 1944), p. 305.
[29] A. K. Faradjian, L. H. Friedman, and D. C. Chrzan, Modell. Simul. Mater. Sci. Eng. **7**, 479 (1999).
[30] M. Verdier, M. Fivel, and I. Groma, Modell. Simul. Mater. Sci. Eng. **6**, 755 (1998).